Petrogenetic grid in the system MgO-SiO2-H2O up to 30 GPa, 1600°C

Petrogenetic grid in the system MgO-SiO_2-H_2O up to 30 GPa, 1600°C: Applications to hydrous peridotite subducting into the Earth's deep interior

Tetsuya Komabayashi, Soichi Omori, and Shigenori Maruyama
Department of Earth and Planetary Sciences, Tokyo Institute of Technology, Tokyo, Japan

Received 24 June 2003; revised 3 November 2003; accepted 26 December 2003; published 25 March 2004.

[1] A semiquantitative petrogenetic grid in the system MgO-SiO_2-H_2O up to 30 GPa and 1600°C was constructed using Schreinemakers analysis on previous experimental data. The grid includes stability relations of hydrous wadsleyite, hydrous ringwoodite, and dense hydrous magnesium silicates (DHMSs): phase A, phase D, phase E, and superhydrous phase B. A sequence of chemical reactions among these hydrous phases was clarified. In the mantle transition zone (410–660-km depth), hydrous wadsleyite and hydrous ringwoodite are stable even at a standard mantle temperature of 1600°C, whereas in the other depths, nominal hydrous phases including DHMSs are stable below 1400°C. Newly found phase transitions in hydrous wadsleyite and hydrous ringwoodite are multiphase and multireaction because their compositions are on neither MgO-SiO_2 nor Mg_2SiO_4-H_2O tie lines, different from single transition in the dry Mg_2SiO_4 system. The grid indicates that water in the subducting slab peridotite would be transported to the bottom of the upper mantle by several DHMSs and hydrous polymorphs of olivine, via solid-solid reactions after antigorite decomposition. Finally, DHMSs would dehydrate to liberate free water at the upper mantle-lower mantle boundary layer or deeper level. We also examined a relation between the predicted depth distributions of dehydration reactions in slab peridotite along several possible pressure-temperature paths and the mode of seismic frequency in each subduction zone. The result suggests a possible origin of intermediate to deep seismicity by the dehydration of hydrous phases in the subducting slab. *INDEX TERMS:* 1025 Geochemistry: Composition of the mantle; 1030 Geochemistry: Geochemical cycles (0330); 1655 Global Change: Water cycles (1836); 7209 Seismology: Earthquake dynamics and mechanics;
KEYWORDS: water transportation, dense hydrous magnesium silicate, deep focus earthquake

Citation: Komabayashi, T., S. Omori, and S. Maruyama (2004), Petrogenetic grid in the system MgO-SiO_2-H_2O up to 30 GPa, 1600°C: Applications to hydrous peridotite subducting into the Earth's deep interior, *J. Geophys. Res.*, *109*, B03206, doi:10.1029/2003JB002651.

1. Introduction

[2] The subduction of oceanic lithosphere drives convection, creating thermal structure and compositional heterogeneities, but most importantly, transporting water into the mantle. The concentration of water in the mantle has significant effects on melting temperatures [e.g., *Kushiro et al.*, 1968; *Iwamori*, 1998], on rheological properties [*Karato et al.*, 1986; *Kohlstedt et al.*, 1996], and on electrical conductivities [*Karato*, 1990; *Li and Jeanloz*, 1991]. In addition to hydrous mid-oceanic ridge basalt (MORB), subducting peridotites (i.e., slab peridotite and down dragged mantle wedge peridotite) are possible water carriers. Numerous experimental attempts were reported to determine the phase relation in a hydrous peridotite system within the deep mantle [*Liu*, 1986; *Kanzaki*, 1991; *Gasparik*, 1993; *Shieh et al.*, 1998; *Irifune et al.*, 1998; *Kuroda and Irifune*, 1998; *Frost and Fei*, 1998; *Frost*, 1999; *Ohtani et al.*, 2000, 2001; *Angel et al.*, 2001; *Ohtani et al.*, 2003]. However, the subsolidus phase relations including hydrous wadsleyite, hydrous ringwoodite, and dense hydrous magnesium silicates (DHMSs) in the hydrous peridotite still remain unknown, because there has been no comprehensive thermodynamic analysis based on Schreinemakers bundle on the experimental results. In addition, most previous experiments were conducted under water-oversaturated conditions which are implausible conditions because free water is likely to penetrate toward the surface from the deep mantle.

[3] Here we present a semiquantitative petrogenetic grid in the system MgO-SiO_2-H_2O (MSH) up to 30 GPa (corresponding to 800-km depth) and 1600°C constructed by Schreinemakers analysis on the previous experimental data. On the basis of this grid, phase changes in the hydrous peridotite and the mechanism of water transportation by the hydrous peridotite down to 800-km depth are discussed. Additionally, a relationship between subduction zone seis-

0148-0227/04/2003JB002651$09.00

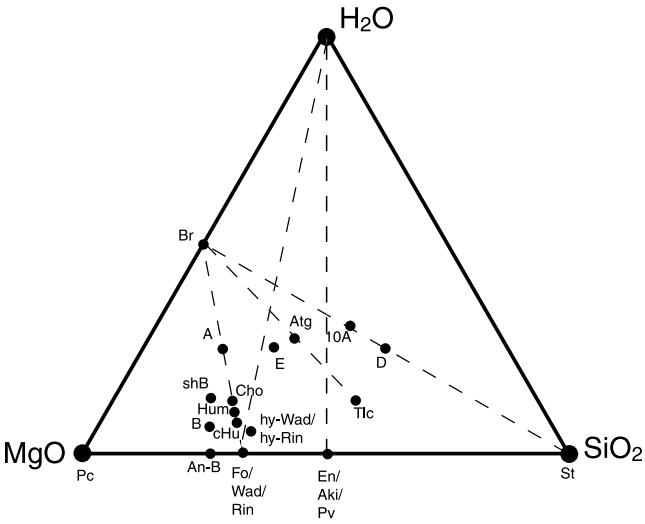

Figure 1. Chemography of the system MgO-SiO_2-H_2O. The phases not described in the text are 10A, 10 angstrom phase; Tlc, talc; Cho, chondrodite; Hum, humite; cHu, clinohumite; B, phase B; and An-B, anhydrous phase B.

micity and dehydration reactions in the slab is considered. The phases are abbreviated as: antigorite (Atg), enstatite (En), forsterite (Fo), phase A (A), phase D (D), phase E (E), superhydrous phase B (shB), stishovite (St), brucite (Br), akimotoite (Aki), magnesium-perovskite (Pv), periclase (Pc), hydrous wadsleyite (hy-Wad), hydrous ringwoodite (hy-Rin), and water (H_2O). The composition of each phase in the ternary MSH system is illustrated in Figure 1 and listed in Table 1.

2. Method (Schreinemakers Bundle)

[4] The phase relations in the ternary MSH system were examined in this study. This model system is a first-order approximation of the hydrous peridotite. Twenty-four mantle phases are known in the model system (Figure 1). In the ternary MSH system, an invariant assemblage is defined by the coexistence of five phases. In combinatorial manner, 42504 ($_{24}C_5$) invariant points and 10626 ($_{24}C_4$) univariant curves are possible. However, some of these assemblages are either metastable or located in negative pressure-temperature (P-T) field. In order to determine the stable assemblages in positive P-T field, previously published experimental results are useful. The previous experimental data determine divariant assemblages at specific P-T conditions, and give constraints on the stability of the combinatorially generated numerous invariant points and univariant curves mentioned above. If the experimental results have consistency with each other, the topologically correct net of the chemical reactions can be located by Schreinemakers analysis.

[5] The experimental results of *Irifune et al.* [1998] and *Ohtani et al.* [2001] were used in this study. They carried out water-oversaturated experiments in the MSH system. Their experimental conditions and results are listed in Table 2. *Irifune et al.* [1998] conducted a series of high-pressure experiments in serpentine bulk composition with 13 wt.% H_2O. *Ohtani et al.* [2000] performed high-pressure experiments in three bulk compositions. The pressure values of *Ohtani et al.* [2000] were reevaluated in their subsequent work [*Ohtani et al.*, 2001]. The results in the systems $MgSiO_3$-15wt.%H_2O and Mg_2SiO_4-11wt.%H_2O of *Ohtani et al.* [2001] with similar water content to that of *Irifune et al.* [1998] were used in this study. We investigated these experimental results to find invariant points. Then, the same reactions from different invariant points were connected. Solid-solid water absent reactions that could not be observed in the water excess original experiments were combined by Schreinemakers rule. Reactions at very low temperature below 500°C were further predicted by extrapolation from high-T phase relations. Since it is difficult for high-pressure experiment to reach equilibrium at such a low-temperature condition, the prediction by Schreinemakers bundle is instructive. By integrating these Schreinemakers nets, we constructed a petrogenetic grid up to 30 GPa (corresponding to 800-km depth) and 1600°C.

[6] Average zero-pressure densities of the phases listed in Table 1 were used to calculate densities of the hydrous peridotite in different P-T conditions. Because there is no

Table 1. Compositions and Zero-Pressure Densities of the Phases

Phase	Composition	Zero-Pressure Density, g/cm^3	Reference
phaseA	$Mg_7Si_2O_8(OH)_6$	2.96	*Horiuchi and Morimoto* [1979]
phaseD	$MgSi_2O_4(OH)_2$	3.50	*Yang et al.* [1997]
phaseE	$Mg_{2.3}Si_{1.28}O_{3.65}(OH)_{2.42}$	3.20	*Kanzaki* [1991]
superhydrous phase B	$Mg_{10}Si_3O_{14}(OH)_4$	3.33	*Pacalo and Parise* [1992]
antigorite	$Mg_{48}Si_{34}O_{85}(OH)_{62}$	2.55	*Robie et al.* [1978]
brucite	$Mg(OH)_2$	2.39	*Fei and Mao* [1993]
enstatite	$MgSiO_3$	3.20	*Fei et al.* [1990]
akimotoite	$MgSiO_3$	3.81	*Fei et al.* [1990]
magnesium-perovskite	$MgSiO_3$	4.10	*Fei et al.* [1990]
forsterite	Mg_2SiO_4	3.22	*Fei et al.* [1990]
dry wadsleyite	Mg_2SiO_4	3.47	*Fei et al.* [1990]
dry ringwoodite	Mg_2SiO_4	3.55	*Fei et al.* [1990]
hydrous wadsleyite[a]	$Mg_{1.89}Si_{0.98}O_{3.7}(OH)_{0.3}$	3.31	*Kudoh et al.* [1996]
hydrous ringwoodite[a]	$Mg_{1.89}Si_{0.98}O_{3.7}(OH)_{0.3}$	3.47	*Inoue et al.* [1998]
periclase	MgO	3.58	*Fei et al.* [1990]
stishovite	SiO_2	4.29	*Fei et al.* [1990]
water	H_2O	1.00	...

[a]Two hydrous polymorphs of olivine are assumed to have the same composition.

Table 2. Previous Experimental Conditions and Results Used in This Study

Pressure, GPa	Temperature, °C	Results[a]
	Irifune et al. [1998]	
6.0[b]	700	Fo + En + Fl
9.0[b]	700	A + En + Fl
10.0[b]	500	A + En
10.0[b]	800	Fo + En + Fl
10.0[b]	1000	Fo + En + Fl
10.0[b]	1100	Fo + En + Fl
11.0[b]	800	A + En + Fl
12.0[b]	700	A + En + Fl
12.0[b]	1100	Fo + En + Fl
13.0[b]	800	E + En + Fl
13.0[b]	1000	E + En + Fl
14.0[b]	700	E + D + Fl
15.0[b]	800	E + D + Fl
15.0[b]	1000	E + En + Fl
16.0[b]	700	A + D + Fl
16.0[b]	1100	E + En + Fl
17.0[b]	800	A + D + Fl
17.0[b]	1000	E + D + Fl
18.0[b]	800	D + shB + Fl
18.0[b]	900	D + shB + Fl
18.0[b]	1000	D + shB + Fl
18.0[b]	1100	E + St + Fl
20.0[b]	600	D + Br
20.0[b]	800	D + shB + Fl
20.0[b]	1000	D + shB + Fl
20.0[b]	1200	hy-Wad + St + Fl
22.0[b]	800	D + shB + Fl
22.0[b]	1000	D + shB + Fl
23.0[b]	1200	hy-Rin + Aki + Fl
25.0[b]	1000	D + shB + Fl
25.0[b]	1200	D + shB + Fl
25.0[b]	1400	Pv + Pc + Fl
26.0[b]	800	D + shB + Br
26.0[b]	1000	D + shB + Fl
26.0[b]	1200	D + shB + Fl
	Ohtani et al. [2001]	
21.0[c]	880	D + shB
21.0[c]	1100	hy-Rin + Fl
21.0[c]	1290	hy-Rin + Fl
23.3[c]	880	D + shB
23.3[c]	1100	D + shB
23.3[c]	1300	hy-Rin + Fl
24.4[c]	880	D + shB + Pv
24.4[c]	1150	D + shB + Fl
24.4[c]	1430	shB + Pv + Fl
21.0[c]	880	D + shB
21.0[d]	880	D + shB
21.0[d]	1300	hy-Rin + Fl
21.0[d]	1370	hy-Rin + Fl
23.3[d]	880	D + shB
23.3[d]	1100	D + shB
23.3[d]	1450	hy-Rin + Fl
24.4[d]	880	D + shB + Pv
24.4[d]	1100	D + shB + Fl
24.4[d]	1320	shB + Pv + Fl

[a]Fo, forsterite; En, enstatite; A, phase A; D, phase D; E, phase E; shB, superhydrous phase B; St, stishovite; hy-Wad, hydrous wadsleyite; hy-Rin, hydrous ringwoodite; Br, brucite; Aki, akimotoite; Pv, magnesium-perovskite; Pc, periclase; Fl, fluid.
[b]In antigorite bulk composition.
[c]In $MgSiO_3$-15wt.% H_2O.
[d]In Mg_2SiO_4-11wt.% H_2O.

available set of equation of state for each high-pressure hydrous phase, discussion on the density of the hydrous peridotite is based on zero-pressure densities only.

[7] Phase D, phase E, hydrous wadsleyite, and hydrous ringwoodite are known to be nonstoichiometric [e.g., *Inoue et al.*, 1995; *Frost*, 1999; *Higo et al.*, 2001]. In addition, fluid at high pressure and temperature could dissolve significant amounts of silicate components [*Irifune et al.*, 1998; *Ohtani et al.*, 2000; *Stalder et al.*, 2001; *Mibe et al.*, 2002]. In this study, however, we assume these phases to have fixed compositions as a first-order approximation (Table 1). We will discuss later the validity of the grid with this assumption. In addition, the limitations for applying the MSH grid in this study to natural multicomponent peridotite will be mentioned.

3. Results

[8] Figure 2 shows the experimental results of *Irifune et al.* [1998] and *Ohtani et al.* [2001]. We constructed a net of chemical reactions consistently with these experiments in Figure 2. Twelve invariant points are found in Figure 2. The P-T positions and Clapeyron slopes of these reactions are restricted by the original experimental data. Since original experiments were conducted under water-oversaturated conditions, most these reactions are water-bearing reactions. Detail Schreinemakers analysis on each invariant point in Figure 2 is shown in Figure 3. One water absent solid-solid reaction originates from each invariant point. The location and Clapeyron slope of predicted solid-solid reaction is loosely constrained by Schreinemakers rule shown as grey area in Figure 3. Chemical reactions found in Figure 2 and Figure 3 intersected with polymorphic phase transition boundaries in Mg_2SiO_4 and $MgSiO_3$ making new invariant points. From these new invariant points, reactions including wadsleyite, ringwoodite, and stishovite occur. Finally, we made a topology of reactions with an internal consistency by connecting the univariant reaction curves. Figure 4 is a petrogenetic grid including all the univariant curves from the invariant points, consisting of 27 invariant points and 78 univariant curves (Table 3).

[9] New phase relations equivalent to the polymorphs of olivine are observed. In this study, both wadsleyite and ringwoodite were assumed to be hydrous with water contents of about 2.0 wt.%. The Mg/Si ratios of these hydrous phases have been known to be less than two [*Inoue et al.*, 1995; *Kudoh*, 2001]. Therefore the compositions of these hydrous olivine polymorphs do not occur on either the Mg_2SiO_4-H_2O or MgO-SiO_2 compositional tie lines (Figure 1), giving rise to a new topology which is different from in the dry Mg_2SiO_4 system. In the hydrous system, the phase boundaries compared to forsterite-wadsleyite transition are the reactions: (15) 15 shB + 77 Fo + 74 En = 200 hy-Wad, (16) 16 E + 101 Fo + 5 En = 129 hy-Wad, and (18) 33 E + 198 Fo = 239 hy-Wad + 2 shB. Note that these reactions are not a single phase transition between forsterite and wadsleyite, but are multiphase and multireaction. The postspinel transformation in the hydrous system is also divided into two hydrous reactions: (65) 100 hy-Rin = 98 Pv + 91 Pc + 15 H_2O (dehydration) and (70) 200 hy-Rin = 15 shB + 151 Pv + 77 Pc (water conserving). These transformations correspond to a single reaction where

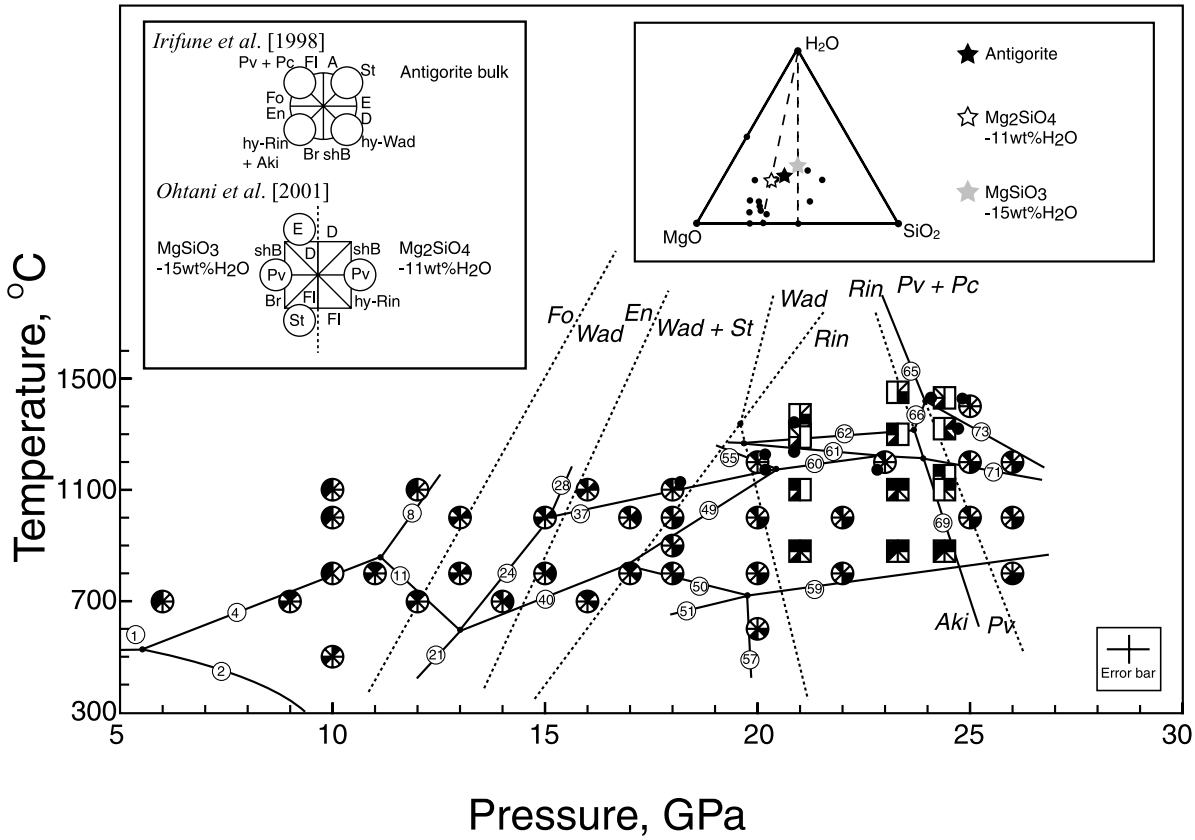

Figure 2. Schreinemakers analysis on the experimental data listed in Table 2. The original data points by *Irifune et al.* [1998] and *Ohtani et al.* [2001] are shown. The star symbol denotes the bulk composition for each experiment. Numbers attached to the reactions correspond to those in Table 3. Phase boundaries in $MgSiO_3$ and Mg_2SiO_4 are from *Fei and Bertka* [1999].

ringwoodite dissociates into magnesium-perovskite and periclase in the dry Mg_2SiO_4 system [*Ito and Takahashi*, 1989]. These two hydrous postspinel transformations intersect to form an invariant point estimated to locate around 24 GPa, 1400°C (Figure 4). Similarly, the reactions enstatite = wadsleyite + stishovite and ringwoodite + stishovite = akimotoite in the dry $MgSiO_3$ system become a combination of reactions in the hydrous system. The former reaction becomes (33) 15 shB + 228 En = 200 hy-Wad + 77 St, (34) 15 D + 174 En = 100 hy-Wad + 106 St, and (35) 145 E + 1878 En = 1170 hy-Wad + 917 St, whereas the latter reaction becomes (54) 300 hy-Rin + 273 St = 567 Aki + 45 H_2O, and (58) 200 hy-Rin + 77 St = 15 shB + 228 Aki.

[10] The phase E-bearing reactions (16) and (35) must be terminated within monomineralic stability field of phase E at about 1300°C. However, no invariant point could be found on these reactions at high temperatures because of a lack of experiment with low water content. Therefore the construction of the phase E-bearing reactions was not completed in the grid.

[11] Figure 5a shows a pseudosection of an assumed bulk composition for the subducting hydrous peridotite. The starting bulk composition is assumed as follows. The subducting hydrous peridotite can be represented by monomineralic serpentinite which consists of antigorite. When the P-T path of the subducting serpentinite intersects the reaction (2) 5 Atg = 14 A + 142 En + 113 H_2O, the mineral assemblage changes to phase A + enstatite + water [*Bose and Ganguly*, 1995; *Ulmer and Trommsdorff*, 1995; *Wunder and Schreyer*, 1997; *Bose and Navrotsky*, 1998]. If the water released by reaction (2) penetrates upward because of its low density, the mineral assemblage in the slab becomes phase A + enstatite, and the bulk water content shifts from 13.0 to 3.7 wt.% [*Frost*, 1999; *Angel et al.*, 2001]. Thus Figure 5 is the pseudosection for water-undersaturated condition, whereas Figure 2 is for water-saturated condition. For the graphical simplicity, the phase relations at temperature below 500°C, i.e., the phase changes along a P-T path passing reaction (6), were not shown in Figure 5.

[12] The shaded area in Figure 5 illustrates where hydrous phases are stable in this bulk composition. At the mantle transition zone (nominally 410–660-km depth), hydrous wadsleyite and hydrous ringwoodite are stable even at a standard mantle temperature of 1500° ~ 1600°C, whereas in the other depths, DHMSs are stable at a relatively low temperature below 1400°C.

[13] Figure 5b shows an average zero-pressure density of phase assemblage for each sector in Figure 5a, approximating a density change of hydrated portion of the subducting peridotite. Major density jump occurs at decomposition of antigorite. After the antigorite breakdown, the density increases by solid-solid reactions during subduction along a cold slab path. The grids in Figure 5 approximate completely serpentinized peridotite. However, it is unlikely

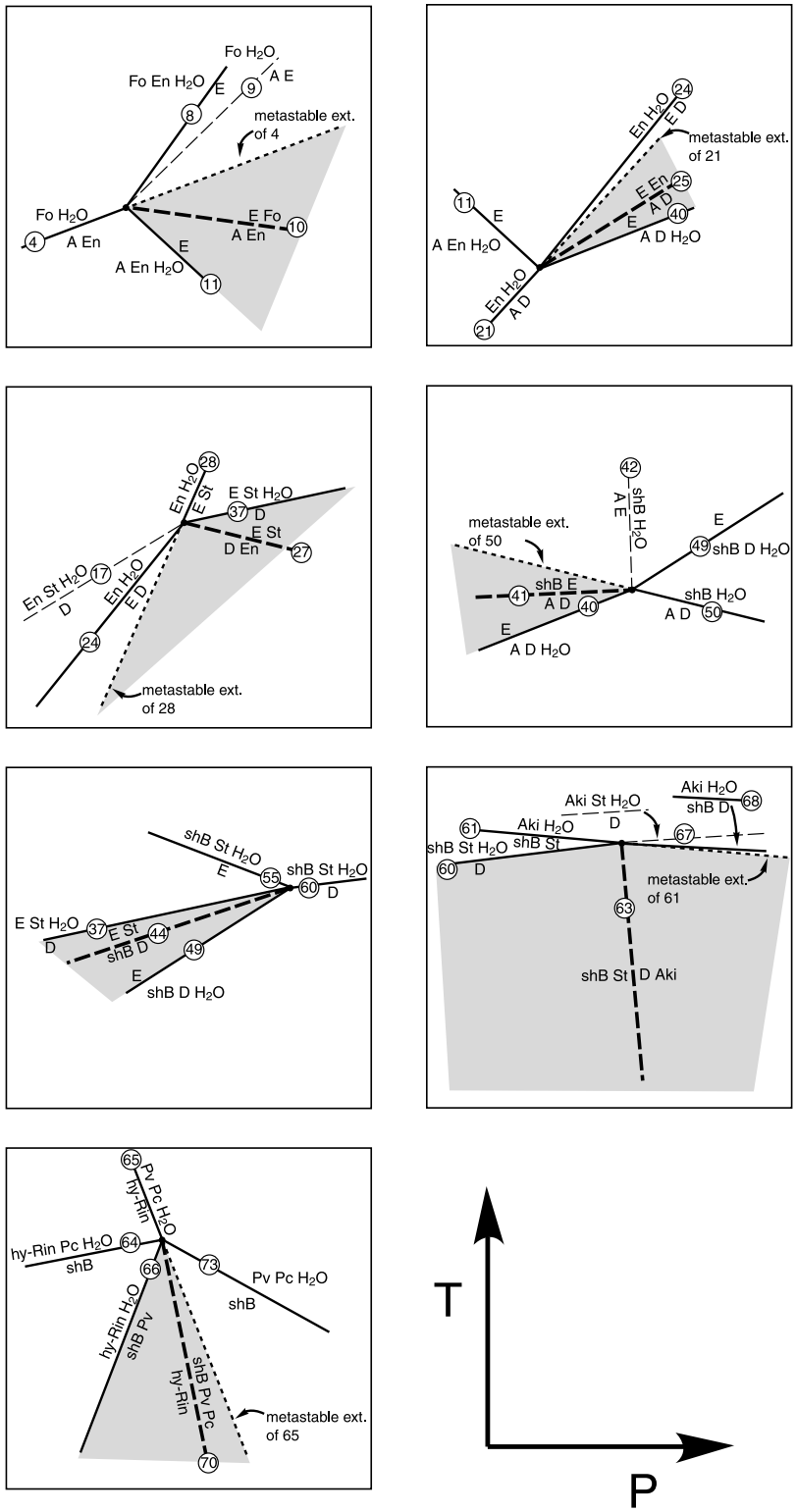

Figure 3. Schreinemakers analysis on selected invariant points found in Figure 2. Solid lines denote the reactions shown in Figure 2, which are constrained by the original experiments of *Irifune et al.* [1998] and/or *Ohtani et al.* [2001]. Dashed lines indicate the reactions predicted from Schreinemakers analysis: thick line, solid-solid reaction; thin line, water-bearing reaction. Numbers attached to the reactions correspond to those in Table 3. Shaded area shows the possible region for each predicted solid-solid reaction to occur.

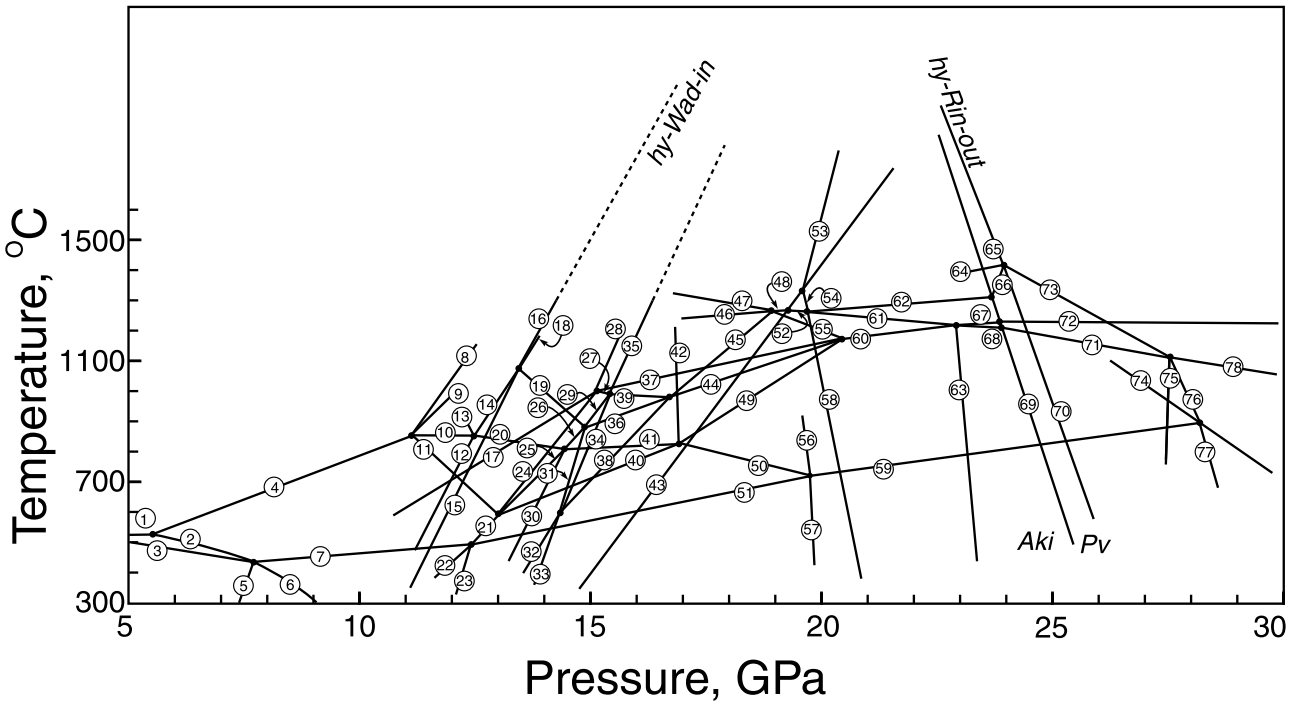

Figure 4. A petrogenetic grid describing all the univariant reactions from the invariant points. Numbers attached to the reactions correspond to those in Table 3.

that the extensive volume of mantle wedge or slab peridotite is totally hydrated. The degree of hydration should be heterogeneous, even though some part may be serpentinized completely. Therefore the densities in Figure 5b must be the minimum value for the natural hydrated peridotite.

4. Discussions

4.1. Validity of the MSH Petrogenetic Grid of This Study

[14] The MSH petrogenetic grid constructed in this study contains numerous solid-solid reactions predicted by Schreinemakers analysis. At the present time, no experiment is available to constrain the locations and the slopes of the predicted reactions. Additionally, we assumed that all the phases to have fixed compositions. In addition, The model MSH system is the first-order approximation of the hydrous peridotite. Here, we discuss the validity of the MSH grid constructed in this study. The limitation of the MSH grid for the discussion in natural multicomponent peridotite is also discussed.

[15] *Irifune et al.* [1998] and *Ohtani et al.* [2001] conducted series of high-pressure experiments with specific bulk compositions. On the basis of the experimental results, they constructed phase diagrams by drawing boundaries between the different mineral assemblages. The boundaries in the phase diagrams were redrawn as chemical reactions and topographical consistency was checked on the basis of Schreinemakers rule in this study. A formation of new higher-pressure DHMS in the water-oversaturated experiments of *Irifune et al.* [1998] and *Ohtani et al.* [2001] is due to a hydration reaction which hardly occurs in the subducting slab. The solid-solid reactions predicted by Schreinemakers analysis, which could not be shown by the original experiments, lead phase changes in the hydrous peridotite (Figure 5). The locations of solid-solid reactions from the invariant points in Figure 2 are constrained by Schreinemakers bundle (Figure 3). In Figure 3, solid-solid reactions (25), (41), (44), and (70) are constrained in their slopes well, and the other solid-solid reactions, (10), (27), and (63), have only loose constraints. The rest of solid-solid reactions from experimentally unconstrained invariant points, which are not found in Figure 2, were not tightly constrained in their locations and slopes. Although the constraints for several solid-solid reactions are not tight, at the present time, our approach is the best method to show a possible solution for the phase relations in the hydrous peridotite, because neither thermodynamic data of DHMSs nor high-pressure experiment is available. Since it has an internal topological consistency, the entire grid in Figure 4 is one possible solution out of the combinatorially generated numerous invariant points and univariant curves as discussed above. Moreover, the density for each sector bounded by the solid-solid reactions in Figure 5b is consistent with the principle of Le Chatelier, i.e., higher-pressure assemblage is always denser with one exception of reaction (14), even though the density values are based on the zero-pressure densities.

[16] The fluid compositions in the experiments of both *Irifune et al.* [1998] and *Ohtani et al.* [2001] were not pure H_2O. At high-P-T conditions, the fluid phase would have contained significant amounts of silicate components, i.e., MgO and SiO_2, as suggested by *Stalder et al.* [2001] and *Mibe et al.* [2002]. Nevertheless, all the topologies in the grid with pure H_2O assumed as a fluid are consistent with the experimental results of both *Irifune et al.* [1998] and *Ohtani et al.* [2001]. This result suggests that the actual

Table 3. Chemical Reactions in the Grid

	Chemical Reaction[a]
(1)	1 Atg = 14 Fo + 20 En + 31 H_2O
(2)	5 Atg = 14 A + 142 En + 113 H_2O
(3)	1 Atg + 71 Br = 17 A + 51 H_2O
(4)	1 A + 3 En = 5 Fo + 3 H_2O
(5)	113 Br + 102 En = 2 Atg + 17 A
(6)	1 Atg = 14 Br + 34 En + 17 H_2O
(7)	5 Br + 2 En = 1 A + 2 H_2O
(8)	100 E = 102 Fo + 26 En + 121 H_2O
(9)	26 A + 300 E = 436 Fo + 441 H_2O
(10)	4 A + 15 En = 10 E + 10 Fo
(11)	102 A + 436 En + 299 H_2O = 500 E
(12)	51 shB + 102 En = 34 A + 187 Fo
(13)	51 A + 97 Fo = 42 shB + 57 E
(14)	121 shB + 536 En = 200 E + 643 Fo
(15)	200 hy−Wad = 15 shB + 77 Fo + 74 En
(16)	129 hy−Wad = 16 E + 101 Fo + 5 En
(17)	1 D = 1 En + 1 St + 1 H_2O
(18)	239 hy−Wad + 2 shB = 33 E + 198 Fo
(19)	32 shB + 150 En = 26 E + 217 hy−Wad
(20)	142 A + 225 En = 243 E + 66 shB
(21)	1 A + 5 D = 12 En + 8 H_2O
(22)	1 D + 1 Br = 2 En + 2 H_2O
(23)	1 A + 1 D = 4 Br + 4 En
(24)	100 E + 102 D = 332 En + 223 H_2O
(25)	12 A + 16 D = 43 E + 1 En
(26)	53 shB + 153 D = 214 E + 191 En
(27)	121 D + 109 En = 100 E + 223 St
(28)	100 E + 102 St = 230 En + 121 H_2O
(29)	3547 hy−Wad + 1508 D = 1686 E + 4334 En
(30)	8 shB + 11 D = 9 A + 28 En
(31)	654 hy−Wad + 56 D = 77 shB + 522 En
(32)	1 shB + 9 St = 2 D + 8 En
(33)	200 hy−Wad + 77 St = 15 shB + 228 En
(34)	100 hy−Wad + 106 St = 15 D + 174 En
(35)	1170 hy−Wad + 917 St = 145 E + 1878 En
(36)	19 shB + 31 D = 56 hy−Wad + 50 E
(37)	230 D = 100 E + 332 St + 109 H_2O
(38)	22 shB + 91 St = 101 hy−Wad + 29 D
(39)	394 hy−Wad + 702 D = 629 E + 985 St
(40)	83 A + 109 D + 5 H_2O = 300 E
(41)	41 A + 52 D = 1 shB + 143 E
(42)	84 A + 14 E = 62 shB + 145 H_2O
(43)	1 hy−Rin = 1 hy−Wad
(44)	109 shB + 750 D = 800 E + 803 St
(45)	247 shB + 565 St = 954 hy−Wad + 290 E
(46)	700 E + 28 shB = 1000 hy−Wad + 753 H_2O
(47)	401 E = 488 hy−Wad + 35 St + 412 H_2O
(48)	189 shB + 413 St = 1000 hy−Wad + 228 H_2O
(49)	67 shB + 119 D + 162 H_2O = 343 E
(50)	17 A + 1 D = 12 shB + 28 H_2O
(51)	1 D + 6 Br = 1 A + 4 H_2O
(52)	189 shB + 413 St = 1000 hy−Rin + 228 H_2O
(53)	567 Aki + 45 H_2O = 360 hy−Wad + 273 St
(54)	300 hy−Rin + 273 St = 567 Aki + 45 H_2O
(55)	100 E = 23 shB + 59 St + 75 H_2O
(56)	26 shB + 13 Br + 52 H_2O = 39 A
(57)	6 shB + 21 D + 3 Br = 12 A
(58)	200 hy−Rin + 77 St = 15 shB + 228 Aki
(59)	3 D + 17 Br = 2 shB + 16 H_2O
(60)	10 D = 1 shB + 17 St + 8 H_2O
(61)	1 shB + 7 St = 10 Aki + 2 H_2O
(62)	13 shB + 59 Aki = 100 hy−Rin + 11 H_2O
(63)	1 shB + 9 St = 2 D + 8 Aki
(64)	98 shB = 300 hy−Rin + 413 Pc + 151 H_2O
(65)	100 hy−Rin = 98 Pv + 91 Pc + 15 H_2O
(66)	13 shB + 59 Pv = 100 hy−Rin + 11 H_2O
(67)	1 D = 1 Aki + 1 St + 1 H_2O
(68)	1 shB + 7 D = 17 Aki + 9 H_2O
(69)	1 Aki = 1 Pv
(70)	200 hy−Rin = 15 shB + 151 Pv + 77 Pc
(71)	1 shB + 7 D = 17 Pv + 9 H_2O
(72)	1 D = 1 Pv + 1 St + 1 H_2O
(73)	1 shB = 3 Pv + 7 Pc + 2 H_2O
(74)	1 Br = 1 Pc + 1 H_2O
(75)	2 D + 9 Pc = 1 shB + 1 Pv
(76)	2 shB = 3 D + 17 Pc + 1 H_2O
(77)	2 shB = 3 D + 1 Br + 16 Pc
(78)	1 D + 1 Pc = 2 Pv + 1 H_2O

[a]Left term is low temperature side of equilibrium boundary. phA, phase A; phD, phase D; phE, phase E; shB, superhydrous phase B; Atg, antigorite; Br, brucite; En, enstatite; Aki, akimotoite; Pv, magnesium-perovskite; Fo, forsterite; hy-Wad, hydrous wadsleyite; hy-Rin, hydrous ringwoodite; Pc, periclase; and St, stishovite.

fluid composition with silicate components does not modify the topology of the grid in the present P-T range. Another problem is the compositions of phase D, phase E, hydrous wadsleyite, and hydrous ringwoodite. The compositions of these hydrous phases in the MSH triangle would depend on the P-T condition [*Inoue et al.*, 1995; *Frost*, 1999; *Higo et al.*, 2001]. The possible compositional ranges of these phases are rather large [e.g., *Frost*, 1999]. The compositional change of these hydrous phases would possibly modify some topologies of the grid constructed in this study.

[17] The petrogenetic grid in this study is in the simple MSH system. Natural peridotite is in the multicomponent system. Addition of iron to the MSH system would change univariant reactions to divariant phase loops because of Mg-Fe substitutions in the phases. Addition of aluminum would produce other phases such as garnet, chlorite, and Mg-sursassite, leading to more complicated phase relations [e.g., *Schmidt and Poli*, 1998; *Frost*, 1999; *Bromiley and Pawley*, 2002]. In particular, majoritic garnet would occur with hydrous wadsleyite, hydrous ringwoodite, or DHMSs at the transition zone [*Frost*, 1999]. Some MSH phases such as antigorite, phase E, and Mg-perovskite can accommodate significant amounts of aluminum [e.g., *Kawamoto et al.*, 1995; *Hirose*, 2002; *Bromiley and Pawley*, 2003], most likely expanding the stability fields of the phases. Humite group minerals were reported in natural peridotitic compositions at high-P-T regions of reaction (4) [*Kawamoto et al.*, 1995; *Stalder and Ulmer*, 2001]. Because clinohumite preferentially accommodate fluorine rather than hydroxyl, the presence of fluorine stabilizes clinohumite [*Stalder and Ulmer*, 2001]. Although the effects of these additional elements on the phase relations would be significant, the following discussions are based on the MSH petrogenetic grid constructed in this study as a first-order approximation. Further experiments in multicomponent system should be done.

[18] Although the present model system is simple compared with the natural system, the grid in this study must have an advance in understanding phase equilibria in the complex stability relations of phases in the mantle, because none of previous reports showed systematic phase relations in the deep hydrous mantle with thermodynamic consistency. The petrogenetic gird in this study is instructive for understanding the phase equillibria of hydrous peridotite, although it is a preliminary and semiquantitative result.

4.2. Water Transportation by Subducting Peridotites

[19] It is suggested that the subducting mantle wedge or slab peridotite is hydrated. The mantle wedge peridotite is

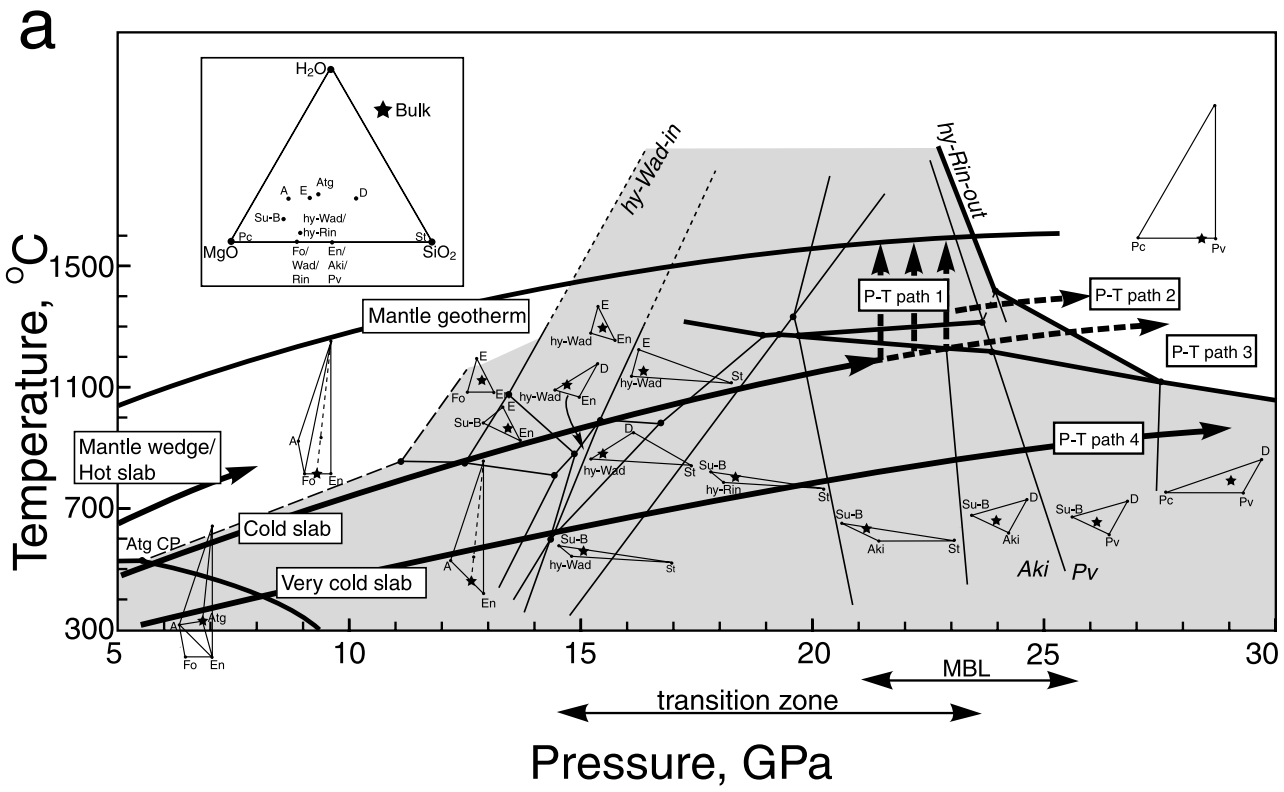
a
Temperature, °C
1500
1100
700
300
5
10
15
20
25
30
Pressure, GPa
H2O
Bulk
MgO
SiO2
Atg
A
E
D
Su-B
hy-Wad/
hy-Rin
Pc
St
Fo/
Wad/
Rin
En/
Aki/
Pv
hy-Wad-in
hy-Rin-out
Mantle geotherm
Mantle wedge/
Hot slab
Cold slab
Very cold slab
Atg CP
P-T path 1
P-T path 2
P-T path 3
P-T path 4
hy-Wad
Fo
En
Fc
Ep
Aki
Pv
MBL
transition zone

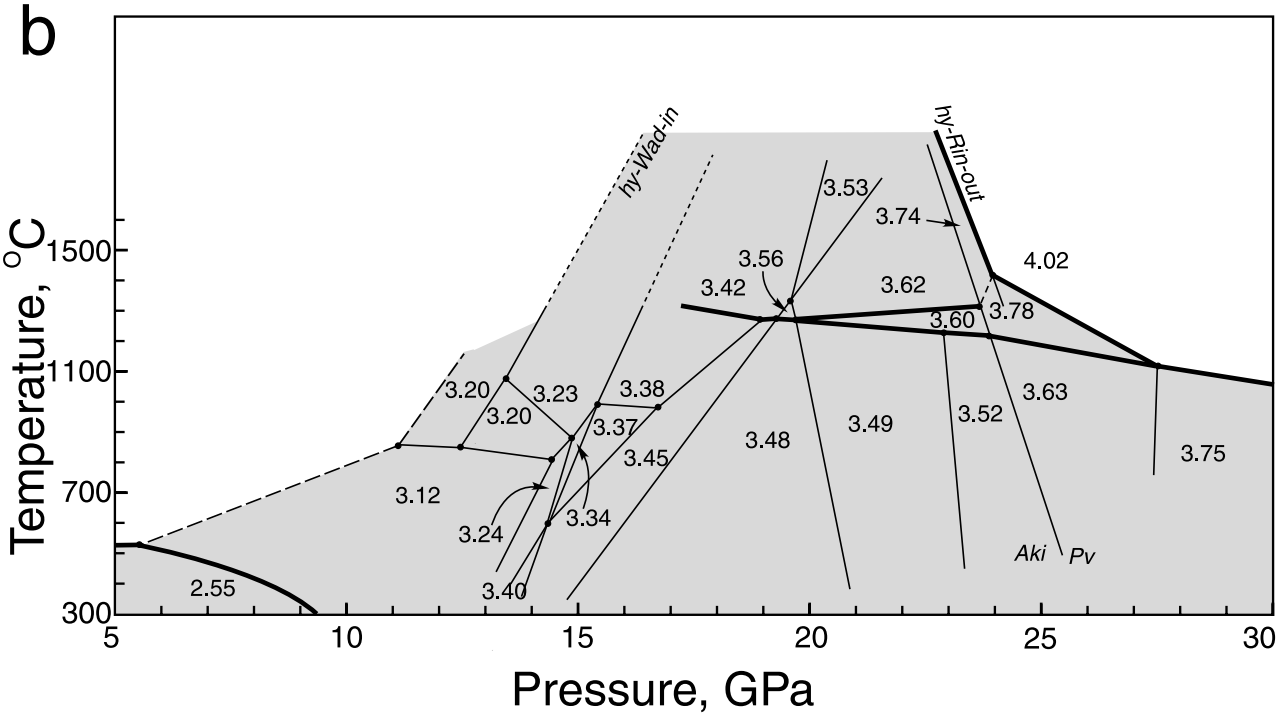
b
Temperature, °C
1500
1100
700
300
5
10
15
20
25
30
Pressure, GPa
hy-Wad-in
hy-Rin-out
2.55
3.12
3.20
3.20
3.23
3.24
3.34
3.37
3.38
3.40
3.42
3.45
3.48
3.49
3.52
3.53
3.56
3.60
3.62
3.63
3.74
3.75
3.78
4.02
Aki
Pv

Figure 5.

believed to be hydrated by water released from the subducting hydrated oceanic crust [e.g., *Poli and Schmidt*, 1995; *Schmidt and Poli*, 1998; *Okamoto and Maruyama*, 1999]. This has been discussed in relations to island arc magmatism [e.g., *Schmidt and Poli*, 1998] and hydrous low-T plume model [*Gerya and Yuen*, 2003].

[20] In contrast, hydration of the subducting slab peridotite has been controversial because there has been neither plausible observation nor mechanical model showing that the slab is hydrated to substantial depth [*Kerrick*, 2002], although recent studies implicitly included hydrated slab peridotite in their water transport models [*Shieh et al.*, 1998; *Irifune et al.*, 1998; *Kuroda and Irifune*, 1998; *Frost and Fei*, 1998; *Frost*, 1999; *Ohtani et al.*, 2000, 2001; *Angel et al.*, 2001]. Substantial hydration of the slab peridotite down to 30–50-km depth from the plate surface was suggested from the consequence to the origin of the double seismic zone observed in the slab, on the basis of the dehydration embrittlement hypothesis [*Seno and Yamanaka*, 1996; *Peacock*, 2001; *Omori et al.*, 2002]. *Omori et al.* [2002] presented a tomographic image of hydrated Pacific plate beneath Tokyo, using the Poisson's ratio as an indicator of serpentinization. Recently, *Ranero et al.* [2003] have discussed the role of bending-related faulting along a trench on the water penetration into the subducting plate to substantial depth. Although the mechanism of hydration is still enigmatic, in the following discussions, it is assumed that the slab peridotite is substantially hydrated as well as the mantle wedge peridotite. In addition, we assume that there is no free fluid coexisting with solid phases.

[21] Water transportation in the hydrous peridotite is discussed by the stability relations of hydrous phases including DHMSs. The hydrous peridotite with phase A + enstatite + water as postantigorite phase assemblage could carry the water into the deep mantle. In addition, Br + En + H_2O assemblage is another possible water carrier in very cold subduction zone (Figure 4). The maximum temperature for the formation of the phase A-bearing assemblage in the subducting peridotite depends on the antigorite choke point as first proposed by *Bose and Ganguly* [1995]. The location of the antigorite choke point is still far from agreement (4–6 GPa, 550°–680°C) [*Ulmer and Trommsdorff*, 1995; *Wunder and Schreyer*, 1997; *Bose and Navrotsky*, 1998; *Bromiley and Pawley*, 2003]. Possible reasons for the discrepancies are the differences in compositions and submicrostructures of antigorites as starting materials and in the methods of high-pressure experiment [*Wunder and Schreyer*, 1997; *Mysen et al.*, 1998; *Bromiley and Pawley*, 2003]. For brucite-bearing assemblage, the required temperature is colder than that for phase A-bearing assemblage (Figure 4).

[22] The mantle wedge and hot slab serpentinites could not clear the antigorite choke point (Figure 5a) [e.g., *Iwamori*, 1998; *Peacock and Wang*, 1999]. Antigorite in the hot P-T path would dehydrate to form dry solid assemblage of Fo + En + H_2O. However, if the water from the subducting MORB layer comes up to the mantle wedge at pressure higher than 10 GPa, phase A or phase E could be formed in the mantle wedge peridotite by reaction (4) or (8), respectively. Then, the water would be transported into deep mantle by the down dragged thin layer (ca. < 10 km) of the mantle wedge peridotite. Lawsonite and phengite in subducting MORB dehydrate at 10 GPa and higher pressure, respectively, if the temperature is below 700°C [*Schmidt and Poli*, 1998; *Okamoto and Maruyama*, 1999].

[23] In contrast, the coldest portion of the slab could clear the critical condition of antigorite choke point for transporting water into the deeper interior [*Iwamori*, 1998; *Peacock and Wang*, 1999; *Omori et al.*, 2004]. Here, we discuss the water transportation by the slab peridotite after antigorite breakdown. For the simplicity, only the phase A-bearing assemblage as postantigorite phases is considered. Figure 5a shows that only solid-solid reactions including DHMSs occur along an assumed P-T path of cold slab down to the mantle boundary layer (MBL: 660 ± 40-km depth) after antigorite breakdown. With increasing pressure, they are reactions (10), (14), (19), (29), (34), (39), (45), (43), and (58). The solid phase assemblages change from antigorite decomposition to A + En, E + Fo + En, E + shB + En, E + hy-Wad + En, D + hy-Wad + En, D + hy-Wad + St, E + hy-Wad + St, shB + hy-Wad + St, shB + hy-Rin + St, shB + Aki + St. The water content of 3.7 wt.% in the slab peridotite does not change during subduction when passing through the upper mantle.

[24] Three P-T paths of the cold subducting slab at MBL are considered in Figure 5a. In P-T path 1, a series of dehydrations occur at MBL: reactions (61) 1 shB + 7 St = 10 Aki + 2 H_2O and (62) 13 shB + 59 Aki = 100 hy-Rin + 11 H_2O. Even though the temperature of slab reaches the standard mantle temperature, hydrous ringwoodite is still a stable hydrous phase. In P-T path 2, another dehydration reaction occurs following reactions (61) and (62). It is reaction (65) 100 hy-Rin = 98 Pv + 91 Pc + 15 H_2O or (73) 1 shB = 3 Pv + 7 Pc + 2 H_2O. This results in the complete dehydration of the slab at the bottom of the upper mantle. In P-T path 3, dehydration reactions (68) 1 shB + 7 D = 17 Aki + 9 H_2O and (73) occur. This P-T path crosses reaction (73) at around 700-km depth. Therefore the free fluid would be released at the top of the lower mantle.

[25] In addition, we consider a very cold slab P-T path (P-T path 4) that gives 900°C at 660-km depth (Figure 5a).

Figure 5. (a) A pseudosection for the bulk composition represented by a star. Standard mantle and several subduction geotherms are shown. Four cold subducting slab geotherms correspond to the slab stagnation at the bottom of the upper mantle (P-T path 1), the avalanche of stagnant slab into the lower mantle (P-T path 2), the slab avalanche into the lower mantle with/without very short time of stagnation (P-T path 3), and the very cold subduction penetrating into the lower mantle (P-T path 4). Shaded area illustrates where hydrous minerals are stable. Atg CP denotes antigorite choke point. Thin and thick solid lines indicate the solid-solid reaction and the dehydration reaction, respectively. Thin dotted line represents water-bearing reactions not occurring in the subduction process. Note, when the geotherm crosses the dehydration reaction, the water content shifts to the lower side indicated by the dotted line in each chemography. See text for details about the bulk composition. (b) Average zero-pressure density of each field. The data of zero pressure of each phase is listed in Table 1.

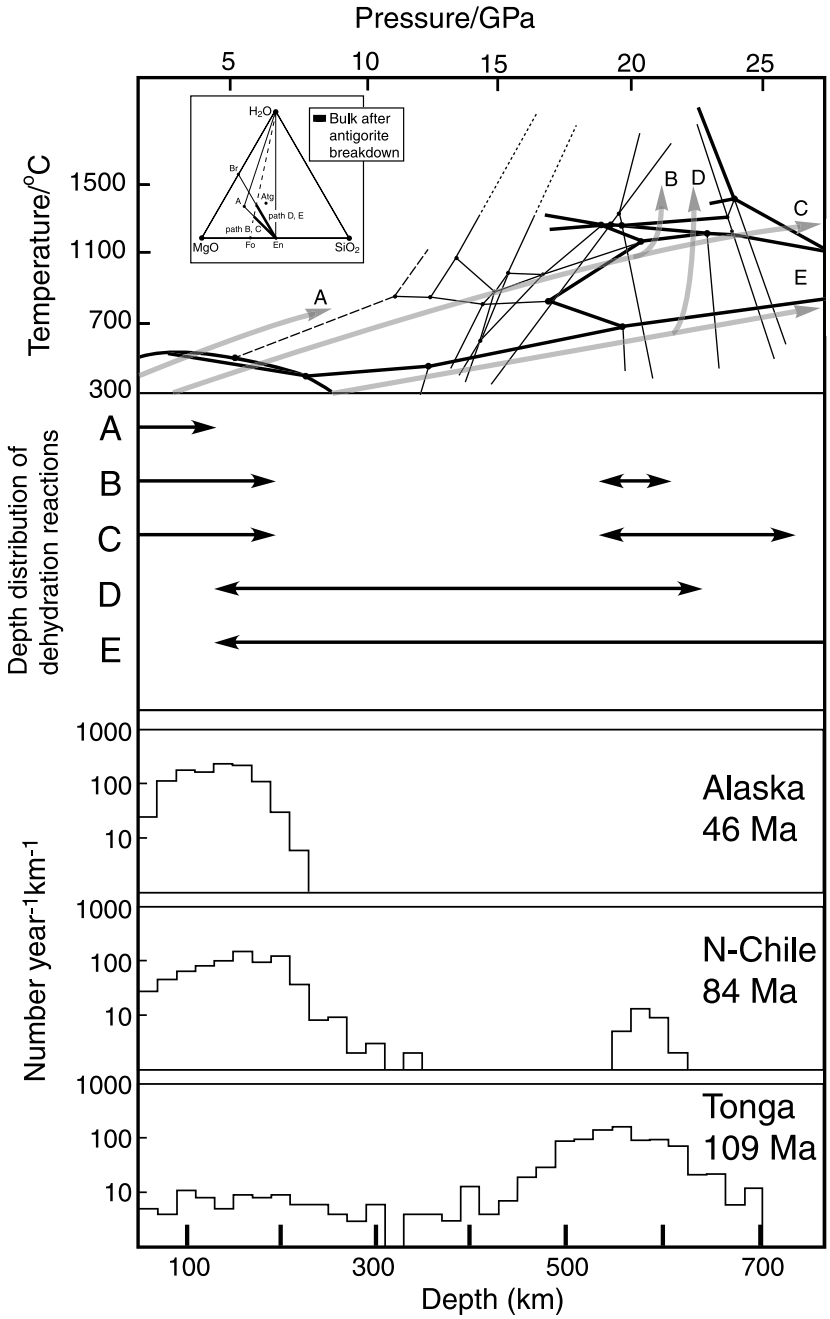

Figure 6. (top) A pseudosection for the bulk compositions represented in the chemography, (middle) the predicted distributions of the dehydration reaction in the slab peridotite along each P-T path (A-E), and (bottom) the frequency mode of seismicity of subduction zone beneath Alaska, northern Chile, and Tonga. The data source for seismic frequency is after *Omori et al.* [2004]. Thin and thick lines in the pseudosection are the same as in Figure 5a. Each P-T path denotes the lowest-T portion in the slab. See text for details.

In this P-T path, the very cold subduction results in no dehydration when entering the lower mantle. This carries water into the middle lower mantle. The first dehydration after antigorite would be reaction (78) 1 D + 1 Pc = 2 Pv + 1 H_2O at around 44 GPa, corresponding to 1100-km depth determined by *Shieh et al.* [1998].

[26] The above case studies of the P-T paths show that possibility for transporting water into the lower mantle strongly depends on dehydration reactions (65), (73), and (78). P-T paths 3 and 4 would carry water into the lower mantle. In P-T paths 1, 2, and 3, two large fluxes of free water from the slab peridotite would occur during subduction down to MBL. These fluxes occur at both the initiation of subduction (antigorite breakdown) and the MBL (DHMSs breakdowns). The free water originating from antigorite would circulate to the surface, sometimes with island arc magmatism [*Ulmer and Trommsdorff*, 1995; *Wunder and Schreyer*, 1997], whereas that from DHMSs

would be bound in wadsleyite and ringwoodite in the mantle transition zone.

4.3. Origin of Seismicity at Deep Subduction Zone

[27] The origin of subduction zone seismicity is one of the central issues of the Earth's dynamics. The origin of the double seismic zone has been discussed in relation to antigorite dehydration [*Seno and Yamanaka*, 1996; *Peacock*, 2001; *Omori et al.*, 2002]. These authors showed that the shape of calculated or experimentally determined antigorite phase diagram plotted on the subduction zone is well consistent with the distribution of seismicity which is double-plane merging as depth increases. *Meade and Jeanloz* [1991] and *Dobson et al.* [2002] reported that antigorite dehydration can generate the earthquake on the basis of the acoustic emission measurements in high-pressure experiments. *Omori et al.* [2002] suggested that dehydration of any hydrous phase could act as a trigger of seismicity. If DHMSs are stable as postantigorite phases in the slab as discussed above, the origin of deep earthquake should be investigated in the light of the dehydration reactions of DHMSs at deep subduction zone.

[28] The depth distribution of the dehydration events predicted from the petrogenetic grid was compared with depth frequency distributions of the earthquakes in Alaska, northern Chile, and Tonga subduction zones (Figure 6). A petrogenetic grid in Figure 6 was drawn for the starting bulk composition on the tie line of brucite and talc with an Mg/Si ratio between Mg_2SiO_4 and $MgSiO_3$, corresponding to a natural serpentinite compositional range containing brucite or talc with predominant antigorite. The released fluid is assumed to escape from the rock. Importantly, in this bulk range, the monomineralic dehydration reactions of phase E and phase D: (49) 343 E = 67 shB + 119 D + 162 H_2O, (55) 100 E = 23 shB + 59 St + 75 H_2O, and (60) 10 D = 1shB + 17 St + 8 H_2O are encountered in addition to the dehydration reactions in Figure 5a. In addition, the very cold subduction passing reaction (6) 1 Atg = 14 Br + 34 En + 17 H_2O is considered, yielding Br + En assemblage as postantigorite phase assemblage (Figure 6).

[29] Five possible P-T paths are considered in Figure 6 (A-E). The path in Figure 6 denotes the lowest-T portion of slab, corresponding to the plate surface at the trench and to the 30–40-km inner portion from the plate surface at MBL. Thus the slab temperature should have a range along the P-T path in Figure 6.

[30] In P-T path A, corresponding to relatively hot (young) subduction, the dehydration reaction in the slab would terminate with antigorite dehydration. Seismic frequency in Alaska may be explained with this depth distribution of dehydration, except for the seismicities deeper than 150 km.

[31] In P-T path B, corresponding to relatively cold (old) subduction with slab stagnation at MBL, the predicted depth distribution of dehydration is bimodal, shallower dehydration by antigorite and deeper dehydrations by DHMSs. The deeper dehydrations would terminate at depth shallower than 660 km because of stagnation of slab. The seismic activity in northern Chile corresponds to this dehydration distribution, except for the seismicities between 200 and 350 km.

[32] P-T path C, similar to path B but without slab stagnation, shows bimodal dehydrations. The deeper dehydration would extend to around 700-km depth. No subduction zone seismicity in the world matches this distribution.

[33] P-T path D corresponding to very cold (old) subduction with slab stagnation, shows dehydration over a wide pressure range, from shallow depth to around 660 km. The Tonga subduction zone seismicity is explainable with this dehydration distribution. On the basis of the P wave velocity structure, *Zhao et al.* [1997] reported that the subducted slab beneath Tonga subduction zone is stagnant at 660-km depth.

[34] In P-T path E, similar to path D but without slab stagnation, the deeper dehydration extends to much deeper, depth around 1000 km or more. No subduction zone seismicity matches this dehydration distribution.

[35] The seismicities deeper than 150 km beneath Alaska and between 200 and 350 km beneath northern Chile are explainable with the dehydration of Mg-sursassite, a hydrous phase in the system MgO-Al_2O_3-SiO_2-H_2O [*Omori et al.*, 2004].

[36] Detailed analyses of this relation in individual subduction zone in the world and in multicomponent systems will be presented by *Omori et al.* [2004]. If dehydration reactions do in fact induce earthquakes in subduction zones, our results show that deep seismicities could be explained by the dehydration hypothesis. Deep seismicity in subduction zones is a possible indicator of water transport into the mantle boundary layer.

[37] **Acknowledgments.** S. Johnson is thanked for his critical improvement on English of the manuscript. The constructive reviews by P. Ulmer, Y. Fei, and anonymous reviewer greatly improved the manuscript. T.K. was supported by the Research Fellowships of the Japan Society for the Promotion of Science for Young Scientists.

References

Angel, R. J., D. J. Frost, N. L. Ross, and R. Hemley (2001), Stabilities and equations of state of dense hydrous magnesium silicates, *Phys. Earth Planet. Inter.*, *127*, 181–196.

Bose, K., and J. Ganguly (1995), Experimental and theoretical studies of the stabilities of talc, antigorite and phase A at high pressures with applications to subduction processes, *Earth Planet. Sci. Lett.*, *136*, 109–121.

Bose, K., and A. Navrotsky (1998), Thermochemistry and phase equilibria of hydrous phases in the system MgO-SiO_2-H_2O: Implications for volatile transport to the mantle, *J. Geophys. Res.*, *103*, 9713–9719.

Bromiley, G. D., and A. R. Pawley (2002), The high-pressure stability of Mg-sursassite in a model hydrous peridotite: A possible mechanism for the deep subduction of significant volumes of H_2O, *Contrib. Mineral. Petrol.*, *142*, 714–723.

Bromiley, G. D., and A. R. Pawley (2003), The stability of antigorite in the systems MgO-SiO_2-H_2O (MSH) and MgO-Al_2O_3-SiO_2-H_2O (MASH): The effects of Al^{3+} substitution on high-pressure stability, *Am. Mineral.*, *88*, 99–108.

Dobson, D. P., P. G. Meredith, and S. A. Boon (2002), Simulation of subduction zone seismicity by dehydration of serpentine, *Science*, *298*, 1407–1410.

Fei, Y., and C. M. Bertka (1999), Phase transitions in the Earth's mantle and mantle mineralogy, in *Mantle Petrology*, edited by Y. Fei, C. M. Bertka, and B. O. Mysen, *Geochem. Soc. Publ.*, *6*, 189–207.

Fei, Y., and H. K. Mao (1993), Static compression of Mg $(OH)_2$ to 78 GPa at high temperature and constraints on the equation of state of fluid H_2O, *J. Geophys. Res.*, *98*, 1875–1884.

Fei, Y., S. K. Saxena, and A. Navrotsky (1990), Internally consistent thermodynamic data and equilibrium phase relations for compounds in the system MgO-SiO_2 at high pressure, *J. Geophys. Res.*, *95*, 6915–6928.

Frost, D. J. (1999), The stability of dense hydrous magnesium silicates in Earth's transition zone and lower mantle, in *Mantle Petrology*, edited by Y. Fei, C. M. Bertka, and B. O. Mysen, *Geochem. Soc. Publ.*, *6*, 283–296.

Frost, D. J., and Y. Fei (1998), Stability of phase D at high pressure and high temperature, *J. Geophys. Res.*, *103*, 7463–7474.

Gasparik, T. (1993), The role of volatiles in the transition zone, *J. Geophys. Res.*, *98*, 4287–4299.
Gerya, T. V., and D. A. Yuen (2003), Rayleigh-Taylor instabilities from hydration and melting propel "cold plumes" at subduction zones, *Earth Planet. Sci. Lett.*, *212*, 47–62.
Higo, Y., T. Inoue, T. Irifune, and H. Yurimoto (2001), Effect of water on the spinel-postspinel transformation in Mg_2SiO_4, *Geophys. Res. Lett.*, *28*, 3505–3508.
Hirose, K. (2002), Phase transitions in pyrolitic mantle around 670-km depth: Implications for upwelling of plumes from the lower mantle, *J. Geophys. Res.*, *107*(B4), 2078, doi:10.1029/2001JB000597.
Horiuchi, H., and N. Morimoto (1979), Crystal structure of $2Mg_2SiO_4 \cdot 3Mg(OH)_2$, a new high-pressure structure type, *Am. Mineral.*, *64*, 593–598.
Inoue, T., H. Yurimoto, and Y. Kudoh (1995), Hydrous modified spinel, $Mg_{1.75}SiH_{0.5}O_4$: A new water reservoir in the mantle transition region, *Geophys. Res. Lett.*, *22*, 117–120.
Inoue, T., D. J. Weidner, P. A. Northrup, and J. B. Parise (1998), Elastic properties of hydrous ringwoodite (γ-phase) in Mg_2SiO_4, *Earth Planet. Sci. Lett.*, *160*, 107–113.
Irifune, T., N. Kubo, M. Isshiki, and Y. Yamasaki (1998), Phase transformations in serpentine and transportation of water into the lower mantle, *Geophys. Res. Lett.*, *25*, 203–206.
Ito, E., and E. Takahashi (1989), Postspinel transformations in the system Mg_2SiO_4-Fe_2SiO_4 and some geophysical implications, *J. Geophys. Res.*, *94*, 10,637–10,646.
Iwamori, H. (1998), Transportation of H_2O and melting in subduction zones, *Earth Planet. Sci. Lett.*, *160*, 65–80.
Kanzaki, M. (1991), Stability of hydrous magnesium silicates in the mantle transition zone, *Phys. Earth Planet. Inter.*, *66*, 307–312.
Karato, S. (1990), The role of hydrogen in the electrical conductivity of the upper mantle, *Nature*, *347*, 272–273.
Karato, S., M. S. Paterson, and J. D. Fitz Gerald (1986), Rheology of synthetic olivine aggregates-influence of grain-size and water, *J. Geophys. Res.*, *91*, 8151–8176.
Kawamoto, T., K. Leinenweber, R. L. Hervig, and J. R. Holloway (1995), Stability of hydrous minerals in H_2O-saturated KLB-1 peridotite up to 15 GPa, in *Volatiles in the Earth and Solar System*, edited by K. A. Farley, pp. 229–239, Am. Inst. of Phys., New York.
Kerrick, D. (2002), Serpentinite seduction, *Science*, *298*, 1344–1345.
Kohlstedt, D. L., H. Keppler, and D. C. Rubie (1996), Solubility of water in the α, β, and γ phases of $(Mg, Fe)_2SiO_4$, *Contrib. Mineral. Petrol.*, *123*, 345–357.
Kudoh, Y. (2001), Structural relation of hydrous ringwoodite to hydrous wadsleyite, *Phys. Chem. Minerals*, *28*, 523–530.
Kudoh, Y., T. Inoue, and H. Arashi (1996), Structure and crystal chemistry of hydrous wadsleyite, $Mg_{1.75}SiH_{0.5}O_4$: Possible hydrous magnesium silicate in the mantle transition zone, *Phys. Chem. Minerals*, *23*, 461–469.
Kuroda, K., and T. Irifune (1998), Observation of phase transformations in serpentine at high pressure and high temperature by in situ X ray diffraction measurements, in *Properties of Earth and Planetary Materials at High Pressure and Temperature*, *Geophys. Monogr.*, vol. 101, edited by M. H. Manghnani and T. Yagi, pp. 545–554, AGU, Washington, D. C.
Kushiro, I., Y. Syonon, and S. Akimoto (1968), Melting of a peridotite nodule at high pressures and high water pressures, *J. Geophys. Res.*, *73*, 6023–6029.
Li, X., and R. Jeanloz (1991), Phases and electrical conductivity of a hydrous silicate assemblage at lower-mantle conditions, *Nature*, *350*, 332–350.
Liu, L.-G. (1986), Phase transformations in serpentine at high pressures and temperatures and implications for subducting lithosphere, *Phys. Earth Planet. Inter.*, *42*, 255–262.
Meade, C., and R. Jeanloz (1991), Deep-focus earthquakes and recycling of water into Earth's mantle, *Science*, *252*, 68–72.
Mibe, K., T. Fujii, and A. Yasuda (2002), Composition of aqueous fluid coexisting with mantle minerals at high pressure and its bearing on the differentiation of the Earth's mantle, *Geochim. Cosmochim. Acta*, *66*, 2273–2285.
Mysen, B. O., P. Ulmer, J. Konzett, and M. W. Schmidt (1998), The upper mantle near convergent plate boundaries, in *Ultrahigh-Pressure Mineralogy*, edited by R. J. Hemley, *Rev. Mineral.*, *37*, 97–138.
Ohtani, E., H. Mizobata, and H. Yurimoto (2000), Stability of dense hydrous magnesium silicate phases in the systems Mg_2SiO_4-H_2O and $MgSiO_3$-H_2O at pressures up to 27 GPa, *Phys. Chem. Minerals*, *27*, 533–544.
Ohtani, E., M. Toma, K. Litasov, T. Kubo, and A. Suzuki (2001), Stability of dense hydrous magnesium silicate phases and water storage capacity in the transition zone and lower mantle, *Phys. Earth Planet. Inter.*, *124*, 105–117.
Ohtani, E., M. Toma, T. Kubo, T. Kondo, and T. Kikegawa (2003), In situ X-ray observation of decomposition of superhydrous phase B at high pressure and temperature, *Geophys. Res. Lett.*, *30*(2), 1029, doi:10.1029/2002GL015549.
Okamoto, K., and S. Maruyama (1999), The high-pressure synthesis of lawsonite in the MORB + H_2O system, *Am. Mineral.*, *84*, 362–373.
Omori, S., S. Kamiya, S. Maruyama, and D. Zhao (2002), Morphology of the intraslab seismic zone and devolatilization phase equilibria of the subducting slab peridotite, *Bull. Earthquake Res. Inst. Univ. Tokyo*, *76*, 455–478.
Omori, S., T. Komabayashi, and S. Maruyama (2004), Dehydration and earthquakes in the subducting slab: Empirical link in intermediate and deep seismic zones, *Phys. Earth Planet. Inter.*, in press.
Pacalo, R. E. G., and J. B. Parise (1992), Crystal structure of superhydrous phase B, a hydrous magnesium silicate synthesized at 1400°C and 20 GPa, *Am. Mineral.*, *77*, 681–684.
Peacock, S. (2001), Are the lower planes of double seismic zones caused by serpentine dehydration in subducting oceanic mantle?, *Geology*, *29*, 299–302.
Peacock, S., and K. Wang (1999), Seismic consequences of warm versus cool subduction metamorphism: Examples from southwest and northeast Japan, *Science*, *286*, 937–939.
Poli, S., and M. W. Schmidt (1995), H_2O transport and release in subduction zones: Experimental constraints on basaltic and andesitic systems, *J. Geophys. Res.*, *100*, 2299–2314.
Ranero, C. R., J. P. Morgan, K. Mclntosh, and C. Reichert (2003), Bending-related faulting and mantle serpentinization at the middle America trench, *Nature*, *425*, 367–373.
Robie, R. A., B. S. Hemingway, and J. R. Fisher (1978), Thermodynamic properties of minerals and related substances at 298, 15 K and 1 bar (10^5 Pascals) pressure and at higher temperature, *U. S. Geol. Surv. Bull.*, *1452*, 456 pp.
Schmidt, M. W., and S. Poli (1998), Experimentally based water budgets for dehydrating slabs and consequences for arc magma generation, *Earth Planet. Sci. Lett.*, *163*, 361–379.
Seno, T., and Y. Yamanaka (1996), Double seismic zones, compressional deep trench-outer rise events, and superplumes, in *Subduction: Top to Bottom*, *Geophys. Monogr. Ser.*, vol. 96, edited by E. Bebout et al., pp. 347–355, AGU, Washington, D. C.
Shieh, S. R., H. K. Mao, R. J. Hemley, and L. Chung Ming (1998), Decomposition of phase D in the lower mantle and the fate of dense hydrous silicates in subducting slabs, *Earth Planet. Sci. Lett.*, *159*, 13–23.
Stalder, R., and P. Ulmer (2001), Phase relations of a serpentine composition between 5 and 14 GPa: Significance of clinohumite and phase E as water carriers into the transition zone, *Contrib. Mineral. Petrol.*, *140*, 670–679.
Stalder, R., P. Ulmer, A. B. Thompson, and D. Günther (2001), High pressure fluids in the system MgO-SiO_2-H_2O under upper mantle conditions, *Contrib. Mineral. Petrol.*, *140*, 607–618.
Ulmer, P., and V. Trommsdorff (1995), Serpentine stability to mantle depths and subduction-related magmatism, *Science*, *268*, 858–861.
Wunder, B., and W. Schreyer (1997), Antigorite: High-pressure stability in the system MgO-SiO_2-H_2O (MSH), *Lithos*, *41*, 213–227.
Yang, H., C. T. Prewitt, and D. J. Frost (1997), Crystal structure of the dense hydrous magnesium silicate, phase D, *Am. Mineral.*, *82*, 651–654.
Zhao, D., Y. Xu, D. A. Wiens, L. Dorman, J. Hildebrand, and S. Webb (1997), Depth extent of the Lau back-arc spreading center and its relation to subduction process, *Science*, *278*, 254–257.

T. Komabayashi, S. Maruyama, and S. Omori, Department of Earth and Planetary Sciences, Tokyo Institute of Technology, 2-12-1 Ookayama, Meguro, Tokyo 152-8551, Japan. (tkomabay@geo.titech.ac.jp)